Computer Methods in Biomechanics and Biomedical Engineering

Publication details, including instructions for authors and subscription information:
http://www.tandfonline.com/loi/gcmb20

Computational modelling of electrocardiograms: repolarisation and T-wave polarity in the human heart

Daniel E. Hurtado [a] & Ellen Kuhl [b c d]

[a] Department of Structural and Geotechnical Engineering, Biomedical Engineering Group, Pontificia Universidad Católica de Chile, Santiago, Chile

[b] Department of Mechanical Engineering, Stanford University, Stanford, CA, 94305, USA

[c] Department of Bioengineering, Stanford University, Stanford, CA, 94305, USA

[d] Department of Cardiothoracic Surgery, Stanford University, Stanford, CA, 94305, USA

Version of record first published: 31 Oct 2012.

To cite this article: Daniel E. Hurtado & Ellen Kuhl (2012): Computational modelling of electrocardiograms: repolarisation and T-wave polarity in the human heart, Computer Methods in Biomechanics and Biomedical Engineering, DOI:10.1080/10255842.2012.729582

To link to this article: http://dx.doi.org/10.1080/10255842.2012.729582

Computer Methods in Biomechanics and Biomedical Engineering
iFirst article, 2012, 1–11

Computational modelling of electrocardiograms: repolarisation and T-wave polarity in the human heart

Daniel E. Hurtado[a]* and Ellen Kuhl[b,c,d]

[a]*Department of Structural and Geotechnical Engineering, Biomedical Engineering Group, Pontificia Universidad Católica de Chile, Santiago, Chile;* [b]*Department of Mechanical Engineering, Stanford University, Stanford, CA 94305, USA;* [c]*Department of Bioengineering, Stanford University, Stanford, CA 94305, USA;* [d]*Department of Cardiothoracic Surgery, Stanford University, Stanford, CA 94305, USA*

(*Received 17 May 2012; final version received 10 September 2012*)

For more than a century, electrophysiologists, cardiologists and engineers have studied the electrical activity of the human heart to better understand rhythm disorders and possible treatment options. Although the depolarisation sequence of the heart is relatively well characterised, the repolarisation sequence remains a subject of great controversy. Here, we study regional and temporal variations in both depolarisation and repolarisation using a finite element approach. We discretise the governing equations in time using an unconditionally stable implicit Euler backward scheme and in space using a consistently linearised Newton–Raphson-based finite element solver. Through systematic parameter-sensitivity studies, we establish a direct relation between a normal positive T-wave and the non-uniform distribution of the controlling parameter, which we have termed refractoriness. To establish a healthy baseline model, we calibrate the refractoriness using clinically measured action potential durations at different locations in the human heart. We demonstrate the potential of our model by comparing the computationally predicted and clinically measured depolarisation and repolarisation profiles across the left ventricle. The proposed framework allows us to explore how local action potential durations on the microscopic scale translate into global repolarisation sequences on the macroscopic scale. We anticipate that our calibrated human heart model can be widely used to explore cardiac excitation in health and disease. For example, our model can serve to identify optimal pacing sites in patients with heart failure and to localise optimal ablation sites in patients with cardiac fibrillation.

Keywords: electrophysiology; depolarisation; repolarisation; electrocardiogram; T-wave; refractoriness; finite element method

1. Introduction

For more than a century, the electrocardiogram has served as a cheap, non-invasive, highly accurate and easily reproducible diagnostic tool to monitor the electrical activity of the human heart. In the healthy heart, the electrocardiogram consists of three characteristic segments: a small hump, the P-wave, associated with atrial depolarisation; a sharp dip-rise-dip sequence, the QRS-complex, associated with ventricular depolarisation; and a small hump, the T-wave, associated with ventricular repolarisation (Noble and Cohen 1978; Keener and Sneyd 1998), see Figure 1. Although the depolarisation sequence and the QRS-complex are relatively well characterised, the repolarisation sequence and the T-wave remain poorly understood (Opthof et al. 2009; Patel et al. 2009). However, the clinical significance of the T-wave cannot be underestimated: inverted T-waves can indicate coronary ischaemia, Wellens' syndrome, left ventricular hypertrophy or central nervous system disorders; tall and narrow symmetrical T-waves can indicate hyperkalaemia; flat T-waves can indicate coronary ischaemia or hypokalaemia (Klabunde 2005). In the healthy heart, the T-wave is positive in all three limb leads. Positive T-waves reflect the fact that the last cells to depolarise are the first to repolarise (Franz et al. 1991). The central hypothesis of this work is that we can incorporate this regional information through a novel non-uniform material parameter, the refractoriness, and that the heterogeneity of this parameter is critical to accurately capture the T-wave profile in the electrocardiogram.

Within the past three decades, computer models of the heart have gained increasing popularity (Clayton et al. 2011). Computer models have the potential to visualise regional depolarisation and repolarisation sequences of the heart (Kotikanyadanam et al. 2010), to localise disturbances (Bacharova et al. 2011), to identify optimal locations for intervention and to virtually probe different treatment options. Conceptually speaking, we can distinguish two classes of electrophysiological models: ionic models and phenomenological models.

Ionic models characterise the electrophysiological behaviour by explicitly considering the transport of charged ions across the cell membrane (MacLachlan et al. 2007; Wong et al. 2011). Their major advantage is that they are mechanistic in origin, providing detailed information

*Corresponding author. Email: dhurtado@ing.puc.cl

ISSN 1025-5842 print/ISSN 1476-8259 online

http://dx.doi.org/10.1080/10255842.2012.729582
http://www.tandfonline.com

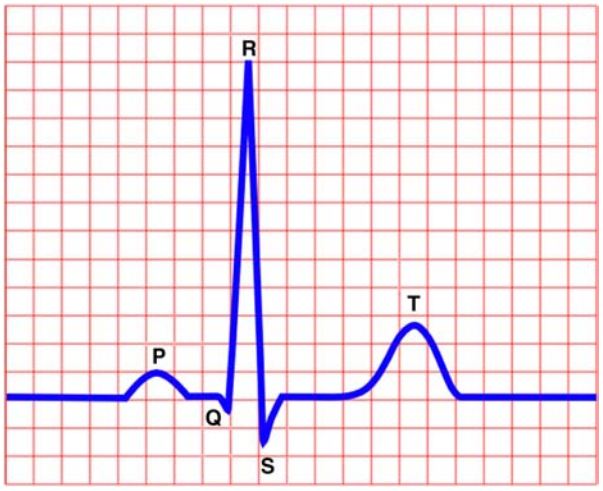

Figure 1. Schematic of electrocardiogram sequence for a healthy human heart, showing the P-wave, QRS-complex and T-wave.

about ion concentrations and ion channel dynamics. However, their inherent disadvantages are their high computational cost and their large number of material parameters. Because of the inherent lack of human tissue samples, the calibration of these parameters is traditionally based on experiments with non-human cells, usually under conditions that barely represent the full physiological regime (Pullan et al. 2005).

Phenomenological models characterise the electrophysiological behaviour by capturing empirical observations on the macroscopic scale. One inherent advantage is their low computational cost. As such, they have played a significant role in advancing the frontiers of computer simulation in cardiac electrophysiology. The majority of cardiac cell models derive from the Hodgkin–Huxley model of the giant squid axon (Hodgkin and Huxley 1952). Simplified two-variable versions of the Hodgkin–Huxley model, e.g. the FitzHugh–Nagumo model (Fitzhugh 1961; Nagumo et al. 1962), have enabled further progress in the mathematical analysis and numerical simulation of cardiac electrophysiology. A modification of the FitzHugh–Nagumo model, the Aliev–Panfilov model for cardiomyocytes (Aliev and Panfilov 1996), has shown excellent agreement with all the salient features of the depolarisation and repolarisation cycle of individual cardiomyocytes, including the dependence of action potential duration on cycle length.

The major disadvantage of phenomenological models is that they typically introduce several material parameters, which lack a direct physiological interpretation. In general, those parameters are calibrated by tuning the proposed model to fit available experimental data. To simplify the calibration process, a common assumption in cardiac electrophysiology is to consider a uniform distribution of the model parameters throughout the entire cardiac domain (Clayton et al. 2011). In reality, however, electrophysiological properties of cardiomyocytes may display large regional variations, sometimes also referred to as dispersion. The observed heterogeneity can be attributed to locally varying densities of gap junctions, ion channels, pumps and exchangers to name but a few (Burton and Cobbe 2001). Spatial heterogeneities give rise to non-uniform conduction velocities and non-uniform action potential durations. Experimental evidence supports the heterogeneity of the action potential duration, both regionally and transmurally (Antzelevitch et al. 1991; Viswanathan et al. 1999; Stoll et al. 2008). In particular, the last regions to depolarise are commonly known to be the first to repolarise, giving rise to positive T-waves in the electrocardiogram (Franz et al. 1987; Cowan et al. 1988; Conrath and Opthof 2006).

Mathematical models of electrophysiology have been solved numerically using finite-difference methods (Panfilov and Keener 1995; Winslow et al. 2000), finite-volume methods (Johnston 2010) and finite-element methods (Rogers and Mc Culloch 1994). In addition to their complete geometric flexibility, finite-element methods have the advantage of seamlessly coupling the primary potential field with other fields, e.g. with a second potential field in bidomain models (Dal et al. 2012), with a mechanical field (Göktepe et al. 2011) in excitation–contraction coupling (Göktepe and Kuhl 2010), or with an optical field in optogenetics (Abilez et al. 2011; Wong et al. 2012). Furthermore, they allow us to use existing finite element infrastructures, e.g. adaptive time stepping schemes, which can reduce the computational time down to the order of minutes or seconds (Wong et al. 2011). Here, we make use of yet another benefit of finite element schemes which comes at almost no additional cost: finite element algorithms allow us to extract computational electrocardiograms in a simple, standard post-processing step (Kotikanyadanam et al. 2010; Bacharova et al. 2011; Okada et al. 2011).

In this study, we use a novel robust, stable and efficient finite element algorithm to systematically explore how the regional variation of cellular action potential profiles affects the repolarisation sequence in a human heart. After briefly summarising the continuous problem of cardiac excitation in Section 2, we illustrate the algorithmic realisation in Section 3. In Section 4, we identify a functional relation between the local action potential duration and a phenomenological model parameter, which we introduce as the *refractoriness*. In Section 5, we utilise this relation to calibrate our model by means of clinically measured action potential durations at different locations in the human heart. We confirm our simulations by computational electrocardiograms which display a normal positive T-wave. Finally, we demonstrate the potential of our model by comparing computationally predicted and clinically measured depolarisation and repolarisation profiles across

the left ventricle. We conclude with a brief discussion and outlook in Section 6.

2. Continuous problem of cardiac excitation

In what follows, we model the excitation of cardiac tissue through a coupled system of equations (Fitzhugh 1961; Nagumo et al. 1962), which characterise the electrical response through the action potential ϕ and the biochemical response through the recovery variable r (Aliev and Panfilov 1996; Göktepe and Kuhl 2009). To account for the propagating nature of excitation waves, we introduce a flux term in the electrical conservation law, while the recovery variable r remains strictly local and governed by local kinetics.

2.1 The global electrical problem

We model the electrical problem through the spatio-temporal evolution of the action potential ϕ, initiated by the flux $\operatorname{div}\mathbf{q}$ and by the source f^{ϕ},

$$\dot{\phi} + \operatorname{div}\mathbf{q}(\phi) = f^{\phi}(\phi, r). \tag{1}$$

The flux term characterises the propagating nature of excitation waves,

$$\mathbf{q} = -\mathbf{D}\cdot\nabla\phi, \tag{2}$$

parameterised in terms of the second-order diffusion tensor $\mathbf{D} = d^{\text{iso}}\mathbf{I} + d^{\text{ani}}\mathbf{n}\otimes\mathbf{n}$, which can account for both isotropic diffusion d^{iso} and anisotropic diffusion d^{ani} along a preferred direction n. The source term characterises the local action potential profile,

$$f^{\phi} = c\phi[\phi - \alpha][1 - \phi] - r\phi, \tag{3}$$

parameterised in terms of a cubic polynomial, $c\phi[\phi - \alpha][1 - \phi]$, and a coupling term, $r\phi$, introducing the recovery variable r. Herein c is a scaling parameter and α is the oscillation threshold. While positive α values characterise stable non-pacemaker cells, negative α values characterise oscillatory pacemaker cells. Experimentally, we can calibrate the global flux term $\mathbf{q}$ using microelectrode array recordings (Chen et al. 2012) and the local source term f^{ϕ} using single-cell patch clamp experiments (Abilez et al. 2011).

2.2 The local biochemical problem

While we assume that the electrical signal ϕ can propagate in space, we model the biochemical problem through the temporal evolution of the recovery variable r, initiated exclusively by the source f^{r},

$$\dot{r} = f^{r}(\phi, r). \tag{4}$$

The source term characterises the slow features of the action potential profile,

$$f^{r} = [\gamma + r\bar{\gamma}(\phi)][-r - c\phi[\phi - b - 1]], \tag{5}$$

parameterised in terms of the weighting factor $[\gamma + r\bar{\gamma}]$ with $\bar{\gamma} = \mu_1/[\mu_2 + \phi]$ and the additional phenomenological parameter b. Parameters μ_1 and μ_2 are essential to calibrate the shape of the restitution curve. In this study, we adopt common parameter values from the literature for the standard FitzHugh–Nagumo parameters c, α and b (Fitzhugh 1961; Keener and Sneyd 1998) and for the non-standard parameters μ_1 and μ_2 (Aliev and Panfilov 1996). In what follows, we focus in particular on parameter γ, its physiological interpretation and its role in cardiac excitation across the scales.

Remark. To simulate physiological values of the transmembrane potential and of the time, it is common to scale the non-dimensional field ϕ and the non-dimensional time t using the following the expressions,

$$\Phi = 100\phi - 80\,\text{mV} \quad \text{and} \quad \tau = 12.9\,\text{tms}.$$

This implies that the transmembrane-potential Φ will range from -80 to $+20$ mV and a typical action potential will last a real time τ of 200–300 ms, which is in agreement with the physiological values for healthy human hearts.

3. Discrete problem of cardiac excitation

For an efficient and robust computational solution of the governing equations (1) and (4), we follow Göktepe and Kuhl (2009) and use a finite difference scheme for time discretisation and a finite element scheme for the spatial discretisation. For the sake of completeness, we summarise the formulation and key aspects of the method in the following. We introduce the action potential ϕ as $\mathcal{C}^0$-continuous global degree of freedom on each finite element node and the recovery variable r as $\mathcal{C}^{-1}$-continuous internal variable on the integration point level. To solve the resulting system of equations, we apply an incremental iterative Newton–Raphson solution strategy, which allows us to adopt an adaptive time stepping scheme (Wong et al. 2011).

3.1 The global electrical problem

On the global level, we transform the electrical problem (1) into its residual format evaluated in domain $\mathcal{B}$, and complement it with the corresponding boundary conditions on the Dirichlet and Neumann boundary $\partial\mathcal{B}_{\phi}$ and

$\partial\mathcal{B}_q$, respectively,

$$R^\phi = \dot{\phi} + \mathrm{div}(\mathbf{q}) - f^\phi = 0 \quad \text{in} \quad \mathcal{B} \tag{6.1}$$

$$\phi = \bar{\phi} \quad \text{on} \quad \partial\mathcal{B}_\phi \tag{6.2}$$

$$\mathbf{q}\cdot\mathbf{n} = \bar{q} \quad \text{on} \quad \partial\mathcal{B}_q. \tag{6.3}$$

By multiplying the residual equation (6.1) by admissible test functions, integrating it over domain $\mathcal{B}$, applying the standard integration by parts and including the Neumann boundary conditions (6.3), we obtain the weak form of the electrical residual. For the spatial discretisation, we discretise the domain of interest $\mathcal{B}$ with n_{el} finite elements $\mathcal{B}_e$ as $\mathcal{B} = \cup_{e=1}^{n_{\text{el}}}\mathcal{B}^e$ and apply the standard isoparametric concept to interpolate the trial functions ϕ^h and the test functions $\delta\phi^h$,

$$\delta\phi^h|_{\mathcal{B}^e} = \sum_{i=1}^{n_{\text{en}}} N^i\,\delta\phi_i \quad \text{and} \quad \phi^h|_{\mathcal{B}^e} = \sum_{j=1}^{n_{\text{en}}} N^j\,\phi_j. \tag{7}$$

Here, N are the standard shape functions on the element level and $i,j = 1,\ldots,n_{\text{en}}$ are the element nodes. For the temporal discretisation, we partition the time interval of interest $\mathcal{T}$ into n_{stp} sub-intervals $[t_n, t_{n+1}]$ as $\mathcal{T} = \cup_{n=0}^{n_{\text{stp}}-1}[t_n, t_{n+1}]$ and apply a standard backward Euler time integration scheme in combination with a finite difference approximation of the first-order time derivative $\dot{\phi}$,

$$\dot{\phi} = \frac{\phi^h - \phi^h_n}{\Delta t}. \tag{8}$$

Here, we have introduced the common abbreviation $\Delta t := t - t_n > 0$ for current time increment. For the sake of clarity, we omit the index $(\circ)_{n+1}$ of the current time point of interest. With the discretisations in space (7) and time (8), the discrete algorithmic residual $\mathtt{R}^\phi_I$ takes the following explicit representation:

$$\mathtt{R}^\phi_I = \mathop{\mathtt{A}}_{e=1}^{n_{\text{el}}} \int_{\mathcal{B}^e} N^i\,\frac{\phi^h - \phi^h_n}{\Delta t} - \nabla N^i\cdot\mathbf{q}\,\mathrm{d}V + \int_{\partial\mathcal{B}^e_q} N^i\,\bar{q}\,\mathrm{d}A - \int_{\mathcal{B}^e} N^i f^\phi \mathrm{d}V \doteq 0. \tag{9}$$

Operator $\mathbf{A}$ symbolises the assembly of all element contributions at the element nodes $i = 1,\ldots,n_{\text{en}}$ to the overall residual at the global node points $I = 1,\ldots,n_{\text{nd}}$. To solve the discrete system of nonlinear equations (9), we apply an incremental iterative Newton–Raphson solution scheme based on the consistent linearisation of the residual (9), which introduces the global iteration matrix,

$$\begin{aligned}\mathtt{K}^\phi_{IJ} &= d_{\phi_J}\mathtt{R}^\phi_I \\ &= \mathop{\mathtt{A}}_{e=1}^{n_{\text{el}}} \int_{\mathcal{B}^e} N^i\,\frac{1}{\Delta t}N^j + \nabla N^i\cdot\mathbf{D}\cdot\nabla N^j \\ &\quad - N^i\,d_\phi f^\phi N^j \mathrm{d}V.\end{aligned} \tag{10}$$

For each incremental iteration step, we update the global vector of unknowns $\phi_I \leftarrow \phi_I - \sum_{J=1}^{n_{\text{nd}}}\mathtt{K}^{\phi\,-1}_{IJ}\mathtt{R}^\phi_J$ at all $I = 1,\ldots,n_{\text{nd}}$ global nodes. In the following sub-section, we illustrate the iterative calculation of the source term $f^\phi(\phi, r)$ required to evaluate the global residual (9) and the calculation of its sensitivity with respect to the action potential ϕ,

$$d_\phi f^\phi = c[-3\phi^2 + 2[1+\alpha]\phi - \alpha] - r - \phi d_\phi r, \tag{11}$$

required to evaluate the global iteration matrix (10). We end this section by noting that all integrals in (9) and (10) are calculated using standard numerical quadrature techniques, where values of ϕ at quadrature points for time $t = t_{n+1}$ result from evaluating the corresponding finite-element interpolation (7).

3.2 The local biochemical problem

On the local level, we introduce the recovery variable r as an internal variable and store it locally at each integration point. For the temporal discretisation, we apply a finite difference approximation

$$\dot{r} = \frac{r - r_n}{\Delta t}, \tag{12}$$

combined with a classical implicit Euler backward time integration scheme. With the discretisation in time (12), the discrete residual $\mathtt{R}^r$ of the recovery equation (4) takes the following representation

$$\begin{aligned}\mathtt{R}^r &= r - r_n - [[\gamma + r\bar{\gamma}][-r - c\phi[\phi - b - 1]]]\Delta t \\ &\doteq 0.\end{aligned} \tag{13}$$

Its consistent linearisation

$$\mathtt{K}^r = d_r\mathtt{R}^r = 1 + [\gamma + \bar{\gamma}[2r + c\phi[\phi - b - 1]]]\Delta t \tag{14}$$

defines the iteration scheme for the incremental update of the recovery variable $r \leftarrow r - \mathtt{K}^{r\,-1}\mathtt{R}^r$ on the integration point level. At local equilibrium, we finally compute the source term f^ϕ from equation (5) for the global electrical problem (9) and its consistent algorithmic linearisation $d_\phi f^\phi$ from Equation (11) for the global Newton iteration (10). To evaluate this linearisation, we calculate the

sensitivity

$$d_\phi r = -[\mathrm{K}^r]^{-1}\partial_\phi \mathrm{R}^r, \tag{15}$$

where K^r is the tangent (14) at local equilibrium, and $\partial_\phi \mathrm{R}^r$ is the sensitivity of the residual,

$$\begin{aligned}\partial_\phi \mathrm{R}^r =&[[\gamma + r\bar{\gamma}]c[2\phi - b - 1] \\ &+ r\partial_\phi\bar{\gamma}[r + c\phi[\phi - b - 1]]]\Delta t,\end{aligned} \tag{16}$$

with $\partial_\phi\bar{\gamma} = -\mu_1/[\mu_2 + \phi]^2$. Within a classical finite element setting, these source and tangent terms are passed to the higher scales, from the biochemical problem (13) and (14) at the integration point level to the electrical problems (9) and (10) at the node point level. Once the global Newton iteration has converged, we store the updated recovery variable r on the integration point level.

4. Local excitation of individual cells

In this section, we study the temporal evolution of the local action potential to gain insight into the excitation of individual cardiac muscle cells. This implies that we can neglect the diffusion term div **q** in (1). The local electrical and biochemical Equations (1) and (4) reduce to the following set of ordinary differential equations,

$$\begin{aligned}\dot{\phi} &= c\phi[\phi - \alpha][1 - \phi] - r\phi \\ \dot{r} &= [\gamma + r\bar{\gamma}(\phi)][-r - c\phi[\phi - b - 1]]\end{aligned}$$

with $\bar{\gamma} = \mu_1/[\mu_2 + \phi]$, which we solve numerically using standard integration schemes. The dynamics of this system and the role of the standard FitzHugh–Nagumo parameters c, α and b have been studied intensely in the past (Fitzhugh 1961; Keener and Sneyd 1998). Here, we have added the non-standard parameters μ_1 and μ_2 to calibrate different restitution curves (Aliev and Panfilov 1996). The additional parameter γ controls the action potential duration. To date, this parameter has not been thoroughly explored, although it plays a critical role in cardiac repolarisation, as we will demonstrate in the sequel. Since the action potential duration directly controls the effective refractoriness of system (Conrath and Opthof 2006), from now on, we will refer to parameter γ as the *refractoriness*.

To quantify the relation between the action potential duration and the refractoriness γ, we solve the local excitation problem and systematically vary the refractoriness γ. In all simulations, we choose $c = 8, \alpha = 0.05$, $b = 0.15, \mu_1 = 0.2, \mu_2 = 0.3$, which are common parameter values for human cardiomyocytes (Aliev and Panfilov 1996; Kotikanyadanam et al. 2010). As initial conditions, we choose $\Phi|_{t=0} = -50\,\mathrm{mV}$ and $r|_{t=0} = 0$, such that the cardiomyocyte is excited with a transmembrane potential slightly above the critical excitation threshold. Figure 2, left, displays the sensitivity of the action potential profile with respect to the refractoriness γ. Despite the inherent nonlinearity of the underlying system of equations, the only property affected by changes in γ is the duration of the action potential itself, while all other features, i.e. the slope of the upstroke, the slope of the recovery and the baseline voltage at the resting stage, remain virtually unchanged. Figure 2, right, displays the corresponding action potential duration APD, i.e. the time until the cardiomyocyte is repolarised by 90%. The curve suggests that the functional relation between APD and γ can be approximated by the following logarithmic expression,

$$\mathrm{APD}_{90} = a_{\mathrm{cell}} + m_{\mathrm{cell}} \cdot \log_{10}(\gamma).$$

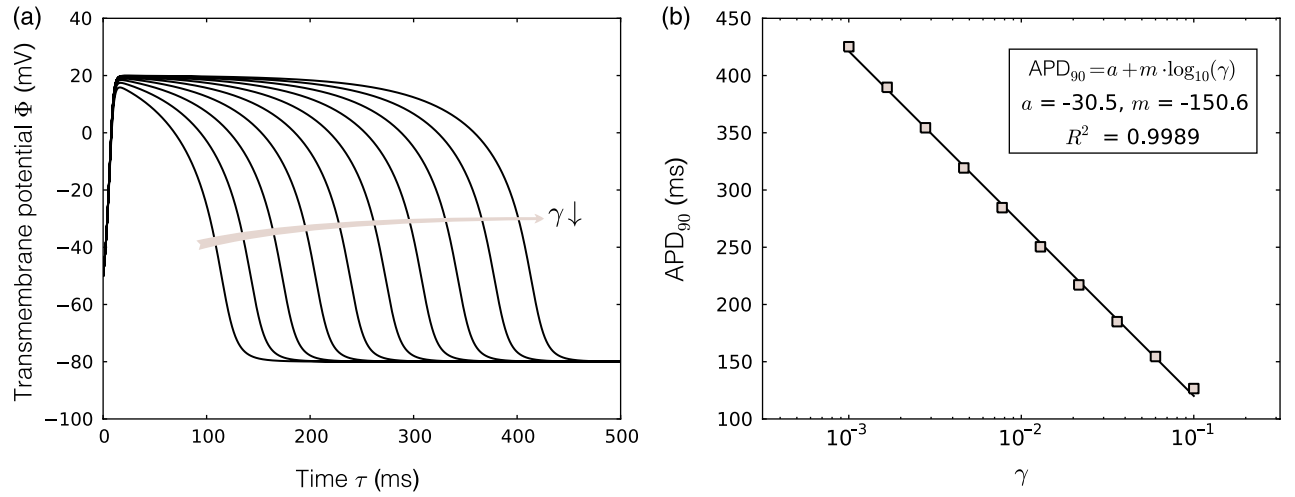

Figure 2. Sensitivity of the action potential profile Φ with respect to the refractoriness γ, left, and functional relation between the action potential duration APD_{90} and the refractoriness γ, right. The refractoriness γ affects the duration of the action potential, but not the slopes of the upstroke, nor the slope of the repolarisation, and neither the baseline voltage at the resting stage.

Using a least-squares linear regression, we obtain the values $a_{\text{cell}} = -30.5$ and $m_{\text{cell}} = -150.6$ for the constants of this model, see Figure 2, right. In further sensitivity studies, we confirmed that these model constants are insensitive to the initial conditions of the boundary value problem.

5. Global excitation of a human heart

Next, we study the spatio-temporal evolution of the action potential to gain insight into the baseline excitation pattern of a human heart. In the healthy heart, the last cells to depolarise are the first to repolarise. As anticipated in Section 1, this characteristic depolariation–repolarisation pattern explains the positive T-wave in normal electrocardiograms. This observation has also been confirmed by electrophysiological studies in human hearts (Cohen et al. 1976; Franz et al. 1987). By mapping the transmembrane potential in different regions of the left and right ventricles, in both the endocardium and epicardium, clinical studies have revealed a linear relation between action potential duration and activation time (Franz et al. 1987; Cowan et al. 1988). This empirical relation can be summarised by the following linear expression,

$$\text{APD}_{90} = a_{\text{heart}} + m_{\text{heart}} \cdot t_{\text{act}}, \tag{17}$$

where t_{act} is the activation time, i.e. the interval between the onset of the QRS-complex and the upstroke of the individual action potential. The constants a_{heart} and m_{heart} are determined from a least-squares fit of expression (17) to the experimental data. Typical values for the slope m_{heart} range from -0.83 to -2.11, with a mean of -1.32 and a standard deviation of 0.45, for healthy patients with positive T-waves (Franz et al. 1987; Cowan et al. 1988).

Motivated by these clinical observations, we partition the geometry of a patient-specific human heart (Kotikanyadanam et al. 2010) into sub-domains according to their activation times. To this end, we solve the global electrical and biochemical equations (1) and (4) described in Section 3 using a finite-element implementation. The elements in the atrioventricular node region are electrically excited, generating wavefronts that travel throughout the entire heart domain. As the initial wavefront propagates, it activates cells in different locations at different times. The time elapsed between the excitation of the elements in the atrioventricular node and the activation of a particular element defines its activation time t_{act}. We then partition the domain into 10 sub-domains and assign each element its corresponding sub-domain according to its local activation time t_{act}, see Figure 3. For each sub-domain, we calculate the average APD_{90} using the empirical relation $\text{APD}_{90} = a_{\text{heart}} + m_{\text{heart}} \cdot t_{\text{act}}$ with $a_{\text{heart}} = 360$ and $m_{\text{heart}} = -1.8$ (Franz et al. 1987; Cowan et al. 1988). For each APD_{90}, we calculate the refractoriness γ using the local equation $\text{APD}_{90} = a_{\text{cell}} + m_{\text{cell}} \cdot \log_{10}(\gamma)$ with $a_{\text{cell}} = -30.5$ and $m_{\text{cell}} = -150.6$. Finally, for each refractoriness γ, we define an individual cell type and assign it to the corresponding sub-domain. In a finite element setting, this assignment is carried out simply via introducing individual material groups, see Figure 3. Table 1 summarises the average activation times t_{act}, the action potential durations APD_{90} and refractoriness parameters γ considered for all 10 sub-domains.

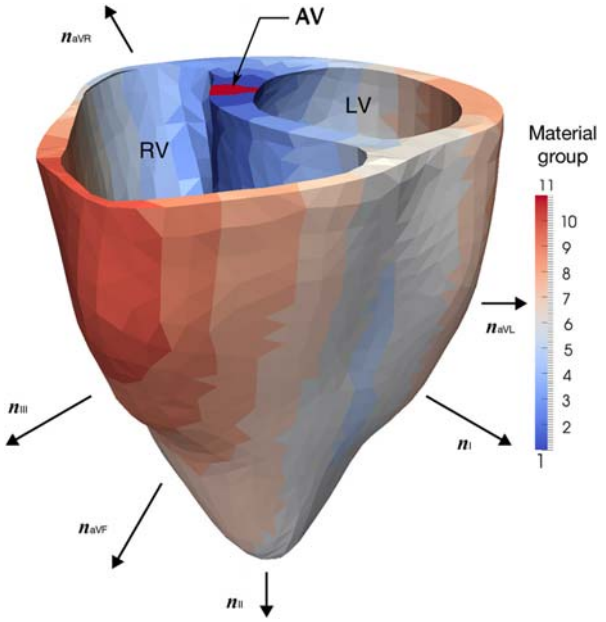

Figure 3. Human heart model partitioned into 10 subregions based on activation times obtained from simulation. The colour code indicates that the dark blue regions depolarise first, whereas the dark red regions depolarise last. In the healthy heart, the regions to depolarise last are the regions to repolarise first. This is modelled through a heterogeneous refractoriness γ with largest values in the red regions and smallest values in the blue regions. Notation: RV represents right ventricle; LV, left ventricle; AV, atrioventricular node; $n_{\text{I}}, n_{\text{II}}, n_{\text{III}}$, limb leads; $n_{\text{aVR}}, n_{\text{aVL}}, n_{\text{aVF}}$, augmented limb leads.

Once the refractoriness is assigned to the different regions in the heart domain, we proceed to solve the electrical propagation problem using the finite element formulation described in Section 3. Parameters c, α, b, μ_1 and u_2 are considered uniform in the domain of analysis, and take the same values reported in Section 4. The isotropic and anisotropic conduction parameters have been set to $d^{\text{iso}} = 2\,\text{mm}^2/\text{ms}$ and $d^{\text{ani}} = 8\,\text{mm}^2/\text{ms}$, respectively. The tetrahedral mesh consists of 11,347 elements and 3129 nodes (Kotikanyadanam et al. 2010), where linear shape functions have been selected as the interpolation basis. We set $\Phi = -80\,\text{mV}$ in the entire domain as initial conditions. Boundary conditions reflect the flux-free condition $\mathbf{q} \cdot \mathbf{n} = 0$ at the domain surface. The time step is set to $\Delta t = 5\,\text{ms}$.

Figure 4 illustrates the action potential profile at different locations in the left ventricle for simulations

Table 1. Regional variation of refractoriness γ in a healthy human heart model.

Material group, region	Average activation time, t_{act} (ms)	Action potential duration, APD_{90} (ms)	Refractoriness, γ
1, 11	7.5	346.5	0.0031
2	17.5	328.5	0.0041
3	27.5	310.5	0.0055
4	37.5	292.5	0.0072
5	47.5	274.5	0.0095
6	57.5	256.5	0.0124
7	67.5	238.5	0.0164
8	77.5	220.5	0.0216
9	87.5	202.5	0.0284
10	97.5	184.5	0.0374

Note: The heart is partitioned into 10 sub-domains. For each sub-domain, we calculate the average activation time t_{act} using the global electrical and biochemical equations. For each activation time t_{act}, we calculate the average APD_{90} using the global equation for the action potential duration. For each APD_{90}, we calculate the refractoriness γ using the local equation for the action potential duration.

considering a uniform and a non-uniform distribution of the refractoriness γ, respectively. In the uniform case shown in Figure 4, left, the action-potential duration is similar for all cardiomyocytes, irrespective of their location and their activation time. In the non-uniform case shown in Figure 4, right, the action-potential duration varies with location and time, in keeping with experimental observations where last regions to depolarise are the first to repolarise. Action potentials in cells immersed in an aggregate can differ from the behaviour of single isolated cells. In particular, one is to expect some differences in the action potential durations for these cases. Since we have established a relation between the refractoriness and APD_{90} based on single-cell simulations, we assessed the error between the target APD_{90} described in Table 1 and the APD_{90} obtained from biventricular simulations. To this end, we computed the APD_{90} from curves in Figure 4, right, and compared them to their corresponding target values in Table 1, and found a maximum relative error of 8%. Thus, we can use activation time, the empirical relation between activation time and action potential duration, and the relation that defines the refractoriness to calibrate our model on the microscopic cell. We will now elaborate how this microscopic calibration translates into clinically relevant macroscopic readouts.

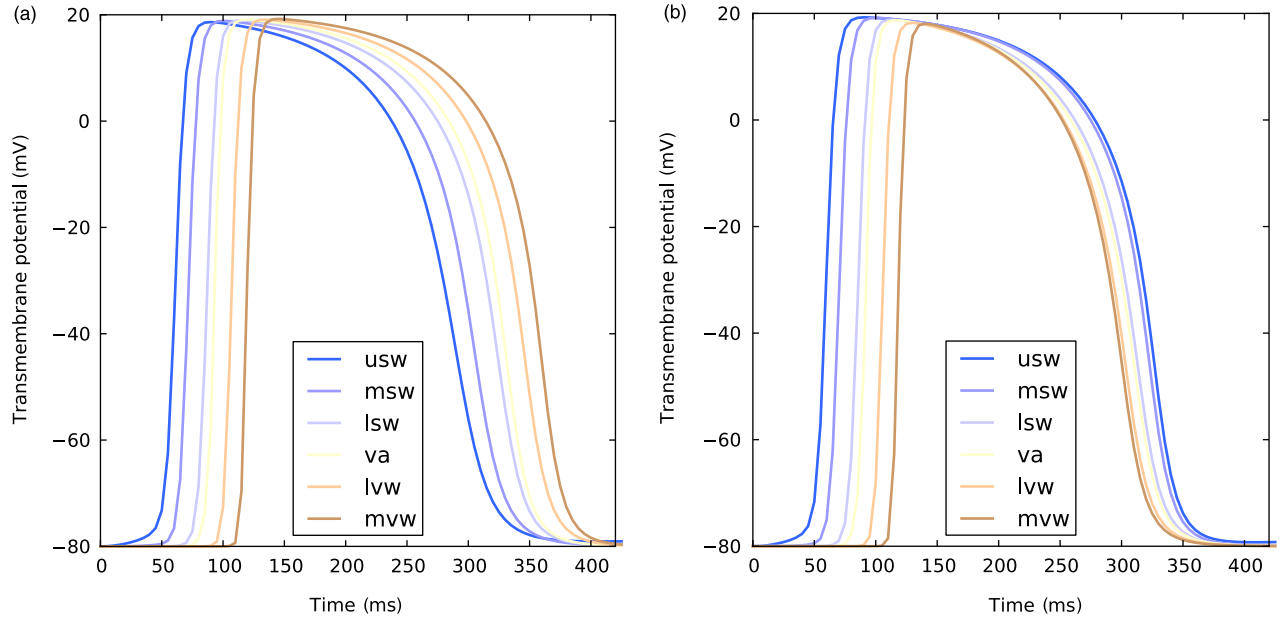

Figure 4. Action potential profiles for seven representative sub-regions in the heart. Uniform distribution of refractoriness γ, left, generates similar action potential profiles at all locations. Non-uniform distribution of refractoriness γ, right, generates spatially varying action potential profiles, where the regions to depolarise last are the regions to repolarise first. Notation: usw represents upper septal wall; msw, mid septal wall; lsw, lower septal wall; va, ventricular apex; lvw, lower ventricular lateral wall; mvw, mid ventricular lateral wall.

Using the non-uniform distribution of the refractoriness γ as summarised in Table 1, we simulate the excitation of a healthy human heart (Kotikanyadanam et al. 2010) based on our fully implicit finite element algorithm (Göktepe and Kuhl 2009). In an additional post-processing step, we compute the electrical flux $\mathbf{q}$ from the diffusion-weighted transmembrane potential gradient $\nabla\phi$, and integrate it numerically over the entire domain to obtain the mean electrical vector $\mathbf{q}$, also known as the *heart vector*,

$$\mathbf{q}^{\heartsuit} = \int_{\mathcal{B}} \mathbf{q}\,\mathrm{d}V \quad \text{with} \quad \mathbf{q} = -\mathbf{D}\cdot\nabla\phi.$$

To calculate the chest electrocardiogram, we project the heart vector $\mathbf{q}^{\heartsuit}$ onto the standard six chest leads (Kotikanyadanam et al. 2010) characterised through the six vectors $\mathbf{n}$ as illustrated in Figure 3,

$$\mathtt{I} = \mathbf{q}^{\heartsuit}\cdot\mathbf{n}_{\mathtt{I}} \qquad \mathtt{II} = \mathbf{q}^{\heartsuit}\cdot\mathbf{n}_{\mathtt{II}} \qquad \mathtt{III} = \mathbf{q}^{\heartsuit}\cdot\mathbf{n}_{\mathtt{III}}$$
$$\mathtt{aVR} = \mathbf{q}^{\heartsuit}\cdot\mathbf{n}_{\mathtt{aVR}} \quad \mathtt{aVL} = \mathbf{q}^{\heartsuit}\cdot\mathbf{n}_{\mathtt{aVL}} \quad \mathtt{aVF} = \mathbf{q}^{\heartsuit}\cdot\mathbf{n}_{\mathtt{aVF}}.$$

The first set of vectors, i.e. the vectors between the left arm and the right arm $n_{\mathtt{I}}$, between the left leg and the right arm $n_{\mathtt{II}}$ and between the left leg and the left arm $n_{\mathtt{III}}$, characterises the limb leads I, II and III. The second set of vectors, i.e. $n_{\mathtt{aVR}}$, $n_{\mathtt{aVL}}$ and $n_{\mathtt{aVF}}$, characterises the augmented limb leads, aVR, aVL and aVF, which are linear combinations of the standard limb leads.

Figure 5, left, displays the electrocardiogram simulated with the uniform parameter distribution according to Figure 4, left. The uniform-parameter model nicely captures the QRS-complex, i.e. the downward–upward–downward sequence at the beginning of the cardiac cycle associated with a normal depolarisation wave. However, the model generates a markedly inverted T-wave, i.e. a negative hump at time $\tau \sim 300$ ms associated with a disturbed repolarisation wave. We conclude that the uniform-parameter model is capable of correctly predicting the depolarisation phase of a healthy human heart, but that it is incapable of correctly predicting the repolarisation phase.

Figure 5, right, displays the electrocardiogram simulated with the non-uniform parameter distribution according to Figure 4, right. The non-uniform-parameter model nicely captures the QRS-complex, i.e. the downward–upward–downward sequence at the beginning of the cardiac cycle associated with a normal depolarisation wave. In contrast to the uniform-parameter model, the non-uniform-parameter model generates a normal T-wave, i.e. a positive hump at time $\tau \sim 300$ ms associated with a normal repolarisation wave. We conclude that the non-uniform-parameter model is capable of correctly predicting the electrophysiology of the healthy human heart, in both the depolarisation and repolarisation phases.

Finally, to validate our model, we compared the sequences of cardiac depolarisation and repolarisation in the lateral left ventricular wall with clinically measured sequences averaged over 10 patients with healthy hearts

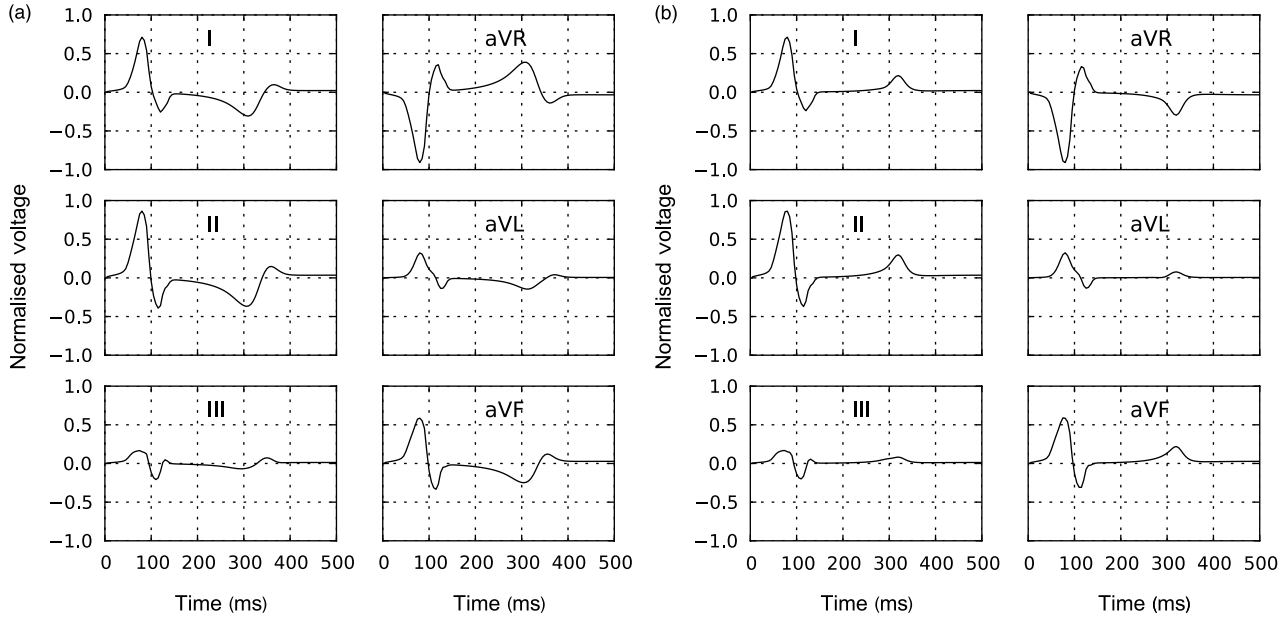

Figure 5. Electrocardiogram for a representative cardiac cycle with limb leads I, II and III and augmented limb leads aVR, aVL and aVF. Uniform distribution of refractoriness γ, left, generates an inverted T-wave, i.e. a negative hump in leads I and II at time $\tau = 300$ ms. Non-uniform distribution of refractoriness γ, right, generates a normal T-wave, i.e. positive hump in leads I and II at time $\tau = 300$ ms. The QRS-complex, i.e. the downward–upward–downward sequence at the beginning of the cardiac cycle, is captured nicely by both models, left and right.

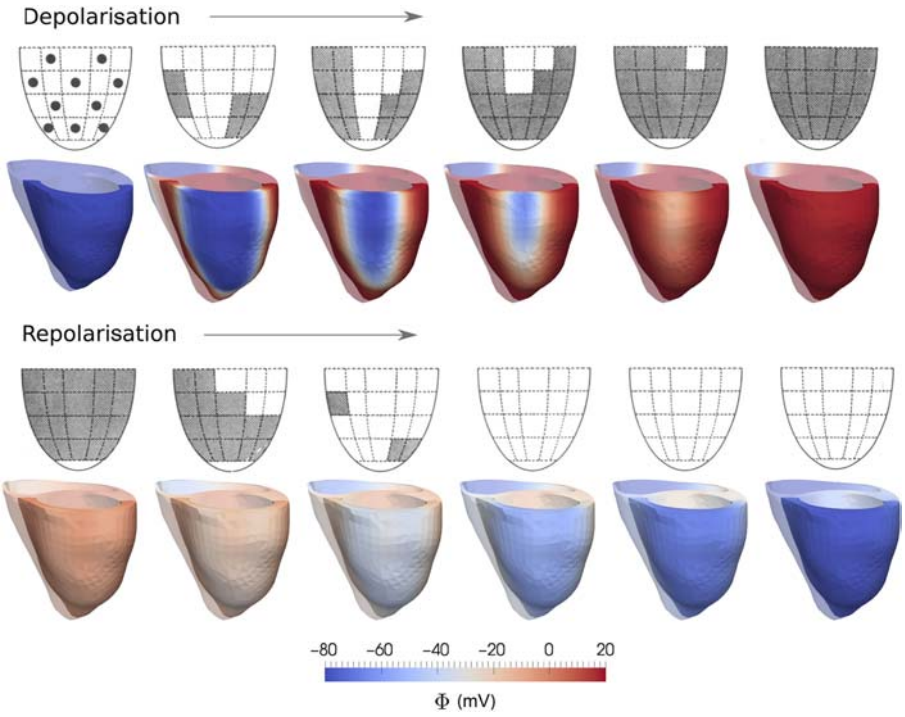

Figure 6. Depolarisation and repolarisation sequences in the healthy human heart. The experimental sequences, top rows, represent the depolarisation and repolarisation of the left ventricle, averaged over 10 healthy individuals, where grey regions indicate activated epicardium; reprinted with permission from Cowan et al. (1988). The computational sequences, bottom rows, represent the depolarisation and repolarisation of a healthy human heart, where the red regions indicate activated myocardium.

and normal T-waves (Cowan et al. 1988). Figure 6 shows the clinically measured and the computationally predicted depolarisation sequences, top row, and repolarisation sequences, bottom row. During the depolarisation phase, the action potential propagates bottom-up and inside-out across the left ventricular free wall. The computational simulations agree nicely with these findings and closely match the clinical excitation pattern. During the repolarisation phase, the action potential returns to its resting state top-down and outside-in. The last regions to depolarise are the first to repolarise. Since the repolarisation time is the sum of activation time and action potential duration, in contrast to the depolarisation pattern, the repolarisation pattern is rather uniform. Again, the computational simulations are in excellent agreement with the clinical observations. Unfortunately, the clinical measurements do not include data on the repolarisation of the septum. Our simulations indicate that the cardiomyocytes in the septal region repolarise later than the cardiomyocytes in the ventricular free walls. Overall, this repolarisation sequence results in the formation of a positive T-wave characteristic for the electrocardiogram of healthy human hearts.

6. Concluding remarks

In the healthy heart, the last cells to depolarise are the first to repolarise. This implies that the action potential durations display significant regional and transmural variations. Here, we reinterpret a phenomenological scaling parameter as the *refractoriness*, and establish a functional relation between the local action potential duration and this material parameter. We then utilise this function to calibrate our model by means of clinically measured action potential durations at different locations in the human heart. Our calibrated model displays the major characteristic features of a healthy human heart; in particular, it correctly reproduces the normal positive T-wave. When mapped across the left ventricle, its depolarisation and repolarisation sequences are in excellent agreement with its clinically measured counterparts.

Transmural variations of action potential durations (Myles et al. 2010; Tsamis et al. 2011) have recently been incorporated into numerical simulations of cardiac electrophysiology to obtain more realistic electrocardiograms (Boulakia et al. 2010). In particular, the experimentally observed linear relation between action potential duration and activation time (Franz et al. 1987) has been successfully integrated into computational models to assure an upright T-wave (Winslow et al. 2000). However, to date, the importance of non-uniform action potential durations has only been recognised phenomenologically, and the regional assignment of the corresponding model parameters has been rather heuristic. Using the concept of a non-uniform refractoriness,

our proposed approach offers an elegant framework to calibrate phenomenological models by means of clinically measured excitation sequences obtained under physiological conditions.

Although the relation between global T-wave polarity and local action potential durations was recognised more than a century ago (Mines 1913), the heterogeneity of cardiac repolarisation remains largely controversial (Opthof et al. 2009; Patel et al. 2009). In particular, the relative contributions of regional and transmural action potential variations to the genesis of a positive T-wave are still a matter of ongoing debate (Bakker and Opthof 2002; Conrath and Opthof 2006). There is strong experimental evidence, which supports that action potential duration and activation time are closely correlated under physiological conditions, irrespective of the location in the heart (Franz et al. 1987; Cowan et al. 1988; Myles et al. 2010). The proposed model could help to further elucidate this hypothesis by using a high-resolution patient-specific model with a non-uniform refractoriness distribution. Numerical simulations would then allow us to study the complex interplay between regional and transmural action potential durations, and assess their role in the formation of positive T-waves in electrocardiograms of healthy individuals (Winslow et al. 2000; Okada et al. 2011). We anticipate that our correctly calibrated baseline model of the human heart has the potential to be widely applicable to explore cardiac excitation profiles in health and disease.

Acknowledgements

This work has been motivated by stimulating discussions with Jonathan Wong, Stanford University, Serdar Göktepe, METU Ankara and Michael Ortiz, Caltech. Their help is gratefully thanked. This research was supported by the Chilean Fondo Nacional de Ciencia y Tecnología (FONDECYT) through Grant #11121224, the National Science Foundation CAREER award CMMI-0952021 and the INSPIRE award CMMI-1233054 and the National Institutes of Health Grant U54 GM072970. DH also acknowledges the support of the Engineering School and the Vicerrectoría Académica of the Pontificia Universidad Católica de Chile through the Fondo de Internacionalización.

References

Abilez OJ, Wong J, Prakash R, Deisseroth K, Zarins CK, Kuhl E. 2011. Multiscale computational models for optogenetic control of cardiac function. Biophys J. 101:1326–1334.

Aliev RR, Panfilov AV. 1996. A simple two-variable model of cardiac excitation. Chaos Solitons Fractals. 7:293–301.

Antzelevitch C, Sicouri S, Litovsky SH, Lukas A, Krishnan SC, Di Diego JM, Gintant GA, Liu DW. 1991. Heterogeneity within the ventricular wall. Circ Res. 69:1427–1449.

Bacharova L, Mateasik A, Krause R, Prinzen FW, Auricchio A, Potse M. 2011. The effect of reduced intracellular coupling on electrocardiographic signs of left ventricular hypertrophy. J Electrocardiol. 44:571–576.

Bakker JMT, Opthof T. 2002. Is the apico-basal gradient larger than the transmural gradient? J Cardiovasc Pharmacol. 39:328–331.

Boulakia M, Cazeau S, Fernández M, Gerbeau J-F, Zemzemi N. 2010. Mathematical modeling of electrocardiograms: a numerical study. Ann Biomed Eng. 38:1071–1097.

Burton FL, Cobbe SM. 2001. Dispersion of ventricular repolarization and refractory period. Cardiovasc Res. 50:10–23.

Chen MQ, Wong J, Kuhl E, Giovangrandi L, Kovacs GTA. 2012. Characterization of electrophysiological conduction in cardiomyocyte co-cultures using co-occurrence analysis. Comput Methods Biomech Biomed Eng., in press, available online first, doi:10.1080/10255842.2011.615310.

Clayton RH, Bernus O, Cherry EM, Dierck H, Fenton FH, Mirabella L, Panfilov AV, Sachse FB, Seemann G, Zhang H. 2011. Models of cardiac tissue electrophysiology: progress, challenges and open questions. Progr Biophys Mol Biol. 104:22–48.

Cohen I, Giles W, Noble D. 1976. Cellular basis for the T wave of the electrocardiogram. Nature. 262:657–661.

Conrath CE, Opthof T. 2006. Ventricular repolarization: an overview of (patho)physiology, sympathetic effects and genetic aspects. Prog Biophys Mol Biol. 92:269–307.

Cowan JC, Hilton CJ, Griffiths CJ, Tansuphaswadikul S, Bourke JP, Murray A, Campbell RW. 1988. Sequence of epicardial repolarisation and configuration of the T wave. Br Heart J. 60:424–433.

Dal H, Göktepe S, Kaliske M, Kuhl E. 2012. A fully implicit finite element method for bidomain models of cardiac electrophysiology. Comput Methods Biomech Biomed Eng. 15:645–656.

Fitzhugh R. 1961. Impulses and physiological states in theoretical models of nerve membrane. Biophys J. 1:445–466.

Franz MR, Bargheer K, Rafflenbeul W, Haverich A, Lichtlen PR. 1987. Monophasic action potential mapping in human subjects with normal electrocardiograms: direct evidence for the genesis of the T wave. Circulation. 75:379–386.

Franz MR, Bargheer K, Costard-Jackle A, Miller DC, Lichtlen PR. 1991. Human ventricular repolarization and T wave genesis. Progr Cardiovasc Dis. 33:369–384.

Göktepe S, Kuhl E. 2009. Computational modeling of cardiac electrophysiology: a novel finite element approach. Int J Numer Methods Eng. 79:156–178.

Göktepe S, Kuhl E. 2010. Electromechanics of the heart - a unified approach to the strongly coupled excitation-contraction problem. Comput Mech. 45:227–243.

Göktepe S, Acharya SNS, Wong J, Kuhl E. 2011. Computational modeling of passive myocardium. Int J Numer Methods Biomed Eng. 27:1–12.

Hodgkin AL, Huxley AF. 1952. A quantitative description of membrane current and its application to conduction and excitation in nerve. J Physiol. 117:500–544.

Johnston P. 2010. A finite volume method solution for the bidomain equations and their application to modelling cardiac ischaemia. Comput Methods Biomech Biomed Eng. 13:157–170.

Keener JP, Sneyd J. 1998. Mathematical physiology: cellular physiology. New York: Springer Verlag.

Klabunde RE. 2005. Cardiovascular physiology concepts. Baltimore: Lippincott Williams & Wilkins.

Kotikanyadanam M, Göktepe S, Kuhl E. 2010. Computational modeling of electrocardiograms: a finite element approach toward cardiac excitation. Int J Numer Methods Biomed Eng. 26:524–533.

MacLachlan MC, Sundnes J, Spiteri RJ. 2007. A comparison of non-standard solvers for ODEs describing cellular reactions in the heart. Comput Methods Biomech Biomed Eng. 10:317–326.

Mines GR. 1913. On functional analysis by the action of electrodes. J Physiol. 46:188–235.

Myles RC, Bernus O, Burton FL, Cobbe SM, Smith GL. 2010. Effect of activation sequence on transmural patterns of repolarization and action potential duration in rabbit ventricular myocardium. Am J Physiol Heart Circ Physiol. 299:H1812–H1822.

Nagumo J, Arimoto S, Yoshizawa S. 1962. An active pulse transmission line simulating nerve axon. Proc IRE. 50:2061–2070.

Noble D, Cohen I. 1978. The interpretation of the T wave of the electrocardiogram. Cardiovasc Res. 12:13–27.

Okada J, Washio T, Maehara A, Momomura S, Sugiura S, Hisada T. 2011. Transmural and apicobasal gradients in repolarization contribute to T-wave genesis in human surface ECG. Am J Physiol Heart Circ Physiol. 301:H200–H208.

Opthof T, Coronel R, Janse MJ. 2009. Repolarization gradients in the intact heart. Circ Arrhythm Electrophysiol. 2:89–96.

Panfilov A, Keener JP. 1995. Re-entry in an anatomical model of the heart. Chaos Solitons Fractals. 5:681–689.

Patel C, Burke JF, Patel H, Gupta P, Kowey PR, Antzelevitch C, Yan G-X. 2009. Cellular basis of the T wave. Circ Arrhythm Electrophysiol. 2:80–88.

Pullan AJ, Buist ML, Cheng LK. 2005. Mathematically modelling the electrical activity of the heart: from cell to body surface and back again. Singapore: World Scientific Publishing Co Pte. Ltd.

Rogers JM, Mc Culloch AD. 1994. A collocation–Galerkin finite element model of cardiac action potential propagation. IEEE Trans Biomed Eng. 41(8):743–757.

Stoll M, Molojavyi MQA, Thämer V, Decking UKM. 2008. Spatial heterogeneity of myocardial perfusion predicts local potassium channel expression and action potential duration. Cardiovasc Res. 77:489–496.

Tsamis A, Bothe W, Kvitting JP, Swanson JC, Miller DC, Kuhl E. 2011. Active contraction of cardiac muscle: in vivo characterization of mechanical activation sequences in the beating heart. J Mech Behav Biomed Mater. 4:1167–1176.

Viswanathan PC, Shaw RM, Rudy Y. 1999. Effects of I Kr and I Ks heterogeneity on action potential duration and its rate dependence: a simulation study. Circulation. 99:2466–2474.

Winslow RL, Scollan DF, Holmes A, Yung CK, Zhang J, Jafri MS. 2000. Electrophysiological modeling of cardiac ventricular function: from cell to organ. Annu Rev Biomed Eng. 2:119–155.

Wong J, Göktepe S, Kuhl E. 2011. Computational modeling of electrochemical coupling: a novel finite element approach towards ionic models for cardiac electrophysiology. Comput Methods Appl Mech Eng. 200:3139–3158.

Wong J, Abilez O, Kuhl E. 2012. Computational optogenetics: a novel continuum framework for the photoelectrochemistry of living systems. J Mech Phys Solids. 60:1158–1178.